A Characterization of TOI-5916b

for the Greater GEMS Survey

Shane O'Brien

Spring 2024

Honors Senior Thesis Submitted to the University of California, Irvine

Submitted Under the Supervision of Professor Paul Robertson

Acknowledgements

I would like to thank my advisor, Professor Paul Robertson, for helping to guide me through this research work and always being so accessible when I needed assistance on either the work itself or the writing process. I would also like to thank Dr. Shubham Kanodia for his time in running the weekly GEMS meetings and for always being willing to help with things as well. Finally, I would like to thank the UCI Department of Physics and Astronomy for the wonderful opportunities they have given me in getting involved in research and for helping me further develop my passion for physics and learning over the last four years.

Contents

1 Introduction 1

1.1 What are Exoplanets? . . . 1

1.2 Exoplanet Detection Methods . . . 3

1.3 What are GEMS? . . . 4

1.4 Project Motivation, Goal & Brief Overview . . . 6

2 Methods 7

2.1 Transit Detection . . . 7

2.2 Radial Velocity (RV) Detection . . . 8

2.3 Markov-Chain Monte Carlo (MCMC) Sampling . . . 9

2.4 `pyexofits` Library . . . 10

3 Data 11

3.1 TESS Instrument Details . . . 11

3.2 TESS Transit Data . . . 12

3.3 HPF Instrument Details . . . 12

3.4 HPF RV Spectroscopy Data . . . 14

4 Results & Analysis 15

4.1 TESS Photometry Fits . . . 15

4.2 HPF RV Fits . . . 17

4.3 Posterior Distribution Values & Analysis . . . 19

5 Discussion 20

5.1 What Can be Learned . . . 20

5.2 Methods for Improvement . . . 20

6 Conclusion 21

7 References 22

1 Introduction

1.1 What are Exoplanets?

The term *exoplanet*, literally meaning "outside planet", came to be the term used to describe planets that were detected/observed outside the solar system [1]. Historically, the first exoplanets were detected in 1992 by the Russian astronomers Aleksander Wolszczan and Dale Frail [2]. They observed two distant, rocky, planets orbiting a pulsar in the constellation Virgo. Even though this system could not harbor life due to the extreme conditions caused by the parent pulsar, this discovery would help give life to this new field of *exoplanet astronomy*.

Several important discoveries involving exoplanets came to light later in the decade and into the next. In 1995, the first exoplanet orbiting a main-sequence star was found [3], then in 1999, the first multi-planet system was detected in the constellation Pegasus [4]. At the turn of the decade, century, and millennium came the most important discovery yet. Astronomers for the first time found an exoplanet in what is known as the *habitable zone* of its host star [5]. When an exoplanet is within this zone, it is the same distance from its host star that Earth is from the Sun, and as such could, in theory, harbor life on its surface, assuming other conditions are not too harsh.

These discoveries led to research in exoplanet astronomy taking off, quite literally. In the early 2000s, the first telescope designed to detect exoplanets was deployed. This telescope was Canada's MOST telescope, MOST meaning *Microvariability and Oscillations of Stars* [6]. This was the first telescope that was designed with the intent of detecting when exoplanets *transit* in front of their host stars [6]. The next telescope to take to the skies was the Spitzer Space Telescope [7]. This was a NASA led infrared telescope whose main purpose was not necessarily to detect exoplanets, but would be used for such work. This was actually the first telescope to directly observe the light from an exoplanet [8].

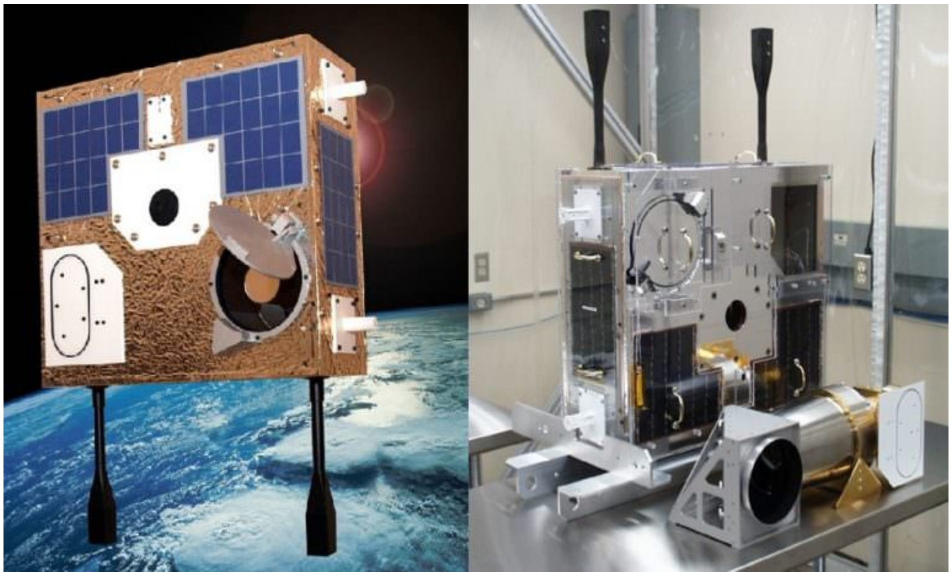

Figure 1: A concept image of the MOST Telescope (left) as well as an image during its construction [9]

As the 2010s rolled around, the next exoplanet hunter would be launched. This telescope being the Kepler Space Telescope [10]. The goal of this telescope was to stare at a patch of sky containing approximately 150,000 stars for a period of four years and look for any stars that have a periodic dip in their brightness [11]. These periodic dips in brightness could correspond to exoplanets orbiting the star. However, due to a malfunction, this telescope ended its primary mission in 2013 [10]. Kepler, however, did make quite a few notable discoveries. It was able to detect the smallest planet, to date, outside the solar system. That being a rocky exoplanet with a radius only 2.2 times greater than that of the Earth. [12]. It also went on to detect and the first Earth-sized exoplanet that existed within its host star's habitable zone [13] [14]. In mid 2014, after Kepler encountered some malfunctions, the mission was started anew under the name K2 as modifications were made to its operation [15]. From here it went on to detect many more exoplanets.

After K2 ran its course, the time called for another new space telescope to detect exoplanets. The new telescope was named TESS, or the *Transiting Exoplanet Survey Satellite* [16]. This telescope was launched in 2018, and is still currently in use. It is the data from this telescope, as well as the ground based *Habitable-Zone Planet Finder* (HPF), that this project used.

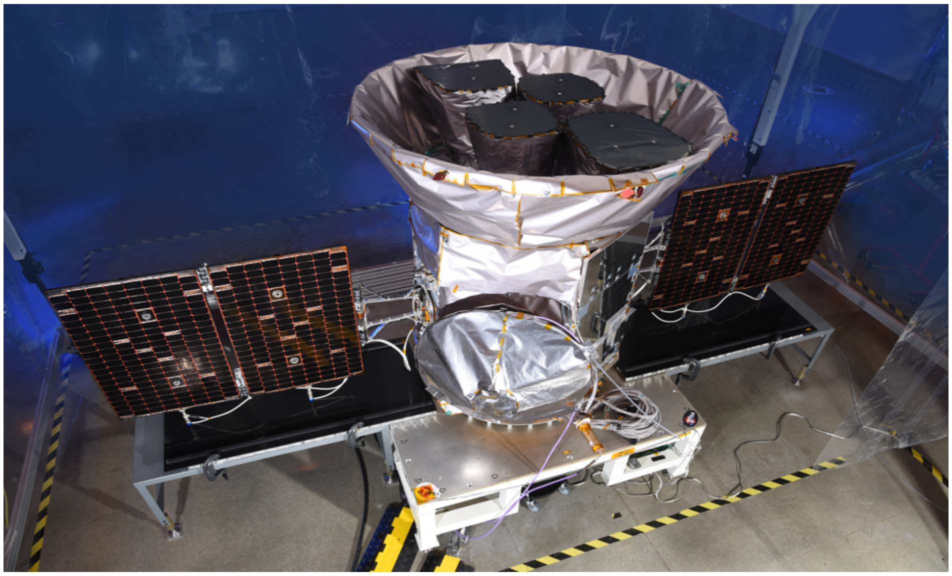

Figure 2: An image of the TESS Telescope prior to launch [17].

The detection and confirmation of exoplanets finally confirmed the long-standing theory that planets do indeed form outside the local solar system. These early discoveries helped usher in a new form of astronomy, that being exoplanet detection, which in turn fueled the need for bigger and better space telescopes over the last thirty plus years.

1.2 Exoplanet Detection Methods

There are many ways to detect exoplanets. One way in which they can be detected, which was briefly mentioned above, is via *transits*. A transit is when an exoplanet passes in front of its host star. A dip in the host star's brightness then occurs, which is then detected by telescopes [18]. If this dip is periodic over some time interval, then that could correspond to an exoplanet being detected. A quantity called the *transit depth* can then be calculated. This value tells the observer if what they are seeing is an exoplanet or something else, however it alone is not the most conclusive method.

Another very popular form of exoplanet detection is the method of *radial velocity shift*. Essentially, when an exoplanet is orbiting its host star, its gravity will pull on the host star, thus causing the star to slightly "wobble" or shift its positions ever so slightly in the direction of our line of sight (i.e. the radial direction). This wobble will cause a Doppler shift in the host star's spectrum [18]. If this Doppler shift, or shift in the radial velocity, of the host star's spectrum is periodic, then it could indicate the presence of an exoplanet. A periodic Doppler shift, such as those observed using this method, can be confirmed to be due to exoplanet signals due to the amplitude of the signal. Since exoplanets are, typically, much smaller than their host stars, the Doppler shift they cause in their host star is much, much smaller than the shift that would be detected if there were a binary companion in the star system.

In addition to these two methods, there are several other detection methods, however, the vast majority of detections have been the result of these methods. The total number of exoplanets found, and through which method, are tabulated below:

Detection Method:	**Number Detected:**
Transit	4,146
Radial Velocity	1,071
Microlensing	204
Imaging	69
Transit Timing Variations	28
Orbital Brightness Variations	9
Pulsar Timing Variations	7
Astrometry	3
Pulsation Timing Variations	2
Disk Kinematics	1

Table 1: A table of all current detections methods and the number of exoplanets detected using each one respectively [18]

1.3 What are GEMS?

GEMS, or *Giant Exoplanets Orbiting M-dwarf Stars*, are the main concern of this work. These are exoplanets that orbit M-type dwarf stars. M-dwarf stars are a particular type of star, where the "M" refers to their spectral classification. M-dwarf stars range in mass anywhere between $0.008M_\odot$ to about $0.6M_\odot$ [19], and range in temperature from about $2,600$K to about $4,000$K [19]. The spectral classification of stars follows the pattern: OBAFGKM. In this sequence, the temperature decreases from left to right. Each spectral classification also has a subclass of 0 through 9, in the same order of decreasing temperature. A table of the stellar classifications is listed below. For reference, the Sun falls into the spectral classification of “G2”.

Type:	O	B	A	F	G	K	M
T_{eff} **(K):**	> 25k	11k – 25k	7.5k – 11k	6k – 7.5k	5.3k – 6k	3.8k – 5.3k	2.2k – 3.8k

Table 2: The stellar classifications and their respective effective temperatures. Each letter classification also has a number classification of 0 through 9 in order of decreasing temperature. The term T_{eff} refers to the temperature of the star’s photosphere, this is the region where the spectrum originates.

So the exoplanets that are the main focus of this work are those that orbit these M-dwarf stars. Why this is of interest is because these M-dwarf stars are, compared to stars similar to our Sun, expected to have lower mass protoplanetary disks, as well as longer Keplerian orbital timescales [19]. The combination of these factors, in theory, makes it quite difficult for giant planets to form around these stars in protoplanetary disks under what is known as the core-accretion formation paradigm.

The core-accretion paradigm, traditionally, has been the idea that when a planet is forming, a rocky core of about $10M_{\oplus}$ must first form. Then, this process is followed by gaseous accretion, which causes the formation of a giant gaseous envelope around the planet. Due to the aforementioned longer orbital time scales and lower mass protoplanetary disks, early studies suggested that the formation of such a massive heavy core, large enough to accrete a gaseous envelope, was not possible due to the lifetime of the gas in the protoplanetary disks. As such, an alternative method of for rapid formation was suggested. This alternative is gravitational instability. Essentially, in this model, a large cloud of gas within the protoplanetary collapses to form these planets, which then can allow for the gas envelope to accrete.

While M-type dwarf stars typically do have several small terrestrial exoplanets within their orbit on average, the occurrence of *giant* exoplanets around these stars is uncertain due to how rare the formation of these stars are [19]. Attempts have been made to understand the occurrence of these *GEMS* exoplanets, however, most studies of this matter have been limited to the case of only using radial velocity data. This is because the Kepler mission, which detected exoplanet transits, only targeted a few M-dwarf stars. However, now with NASA’s TESS exoplanet telescope, which has all-sky coverage, observing M-dwarf transits is much easier. Despite the fact that GEMS should have quite a low formation rate, the TESS telescope has been able to identify enough transiting GEMS that it is now possible to attempt to characterize the occurrence rate of these transiting GEMS [19].

1.4 Project Motivation, Goal & Brief Overview

The purpose of this project to help aid in the larger scientific endeavor of characterizing the occurrence of these GEMS systems. This will be done by focusing in on the individual GEMS candidate, TOI-5916, and doing analysis work in order to confirm its nature as a GEMS system and characterize its parameters. This analysis work, in conjunction with the greater GEMS survey project, will help to provide better constraints on the occurrence rate and physical properties of GEMS.

This study will utilize both transit data from the TESS space telescope, and radial velocity (RV) data from the ground-based HPF instrument at the McDonald Observatory in Texas. Data from these instruments will then be analyzed to characterize the system TOI-5916b, with the help of Markov-Chain Monte Carlo simulations to help with the curve fitting processes.

2 Methods

2.1 Transit Detection

As discussed in section 1, one of the two main methods of exoplanet detection is through a process called *transit photometry.* In a basic sense, a telescope, such as TESS, observes several stars over a long period of time and looks for dips in their brightness. Periodic dips in brightness could correspond to a planet orbiting in front of a star. Sounds simple, however a more detailed discussion of the mathematics behind this observation method is justified.

We start by looking at a quantity known as the *transit depth.* This is defined as the fraction of light blocked as the exoplanet crosses in front of the star. Mathematically, this is defined as:

$$\frac{\Delta f}{f} = \left(\frac{A_{pl}}{A_*}\right) = \left(\frac{R_{pl}}{R_*}\right)^2 \tag{1}$$

This dip in the star's brightness can be easily observed from the *light curve.* The light curve is a measure of flux of the star over time. Once an exoplanet transits, a noticeable dip in the light curve will become present.

Thus, from a measurement as simple as the transit depth, the radius of the planet can be measured using:

$$R_{pl} = R_* \sqrt{\frac{\Delta f}{f}} \tag{2}$$

The orbital distance to the host star can also be calculated. This is done via Kepler's 3rd Law, which is mathematically shown as:

$$P^2 = \frac{4\pi^2 a^3}{G(M_{pl} + M_*)} \tag{3}$$

In the exoplanet limit, where $M_{pl} \ll M_*$, we have:

$$a^3 \approx \frac{GM_* T^2}{4\pi^4} \tag{4}$$

In these equations, T is the period of the planet's orbit around the star, and a is the length of the semi-major axis of the ellipse, which is the same as the orbital distance.

2.2 Radial Velocity (RV) Detection

It should be noted that the process of calculating the radius of the host star, r_*, is another process entirely, and can be calculated by analyzing the luminosity of the host star as well as its distance from us, the observers which can be done, for instance, via the method of parallax.

The other main way of detecting exoplanets is via the *radial velocity* method, or RV method for short. In a basic sense, observations with the RV method looks for Doppler shifts in the star's spectral lines. This is done via analyzing the star's light with a spectrograph and analyzing the results relative to some baseline spectrum to look for shifts.

In essence, this method is governed by the Doppler shift, which in a simple case is given by:

$$\frac{v_r}{c} = \frac{\Delta\lambda}{\lambda_0} = \frac{\lambda_{obs} - \lambda_0}{\lambda_0} \tag{5}$$

Where λ_{obs} refers to the observed wavelength of light and λ_0 refers to the emitted wavelengths of light. Then the term v_r is the radial velocity of the star. Essentially, just as is the case for sound, when a wave source is moving towards you, the waves you observe are shorter than when the source is stationary, and when the source is moving away from you, the observed waves are longer than when the source is stationary.

The radial velocity of a star is defined as the component of the velocity along the star's line of motion with the observer. This is better shown in the diagram below.

As the exoplanet pulls on the star, via Newton's 3rd Law, this causes the star to move back and forth in a sort of "wobble". This wobble is then detected via analyzing the spectrum and looking for these shifts.

We can also define the radial velocity in terms of it being a component of the proper motion of the star, that is, the observed speed of the star in the sky. In a visual sense, we define this as:

It is thus common to refer to the radial velocity by the term k, which in this context refers to the radial velocity of the star, *not* the exoplanet. We define k as:

$$k = |v| \sin(i) \tag{6}$$

Where, $|v|$ is the amplitude of the proper motion of the star, and i is the angle of inclination relative to the observer.

In the case where the exoplanet also transits the star, then the inclination angle of the planet can be found, from which the mass of the exoplanet can be found. This can be done via the following equation, where as usual we take M_{pl} to be the mass of the planet, and M_* to be the mass of the host star:

$$\frac{Tk}{2\pi G} = \frac{M_{pl}^3}{(M_* + M_{pl})^2} \sin^3(i) \tag{7}$$

In the limit where $M \gg M_{pl}$, which is usually the case in exoplanet detection, we can simplify the above relation to the following:

$$M_{pl} \sin(i) \approx \left(\frac{T}{2\pi G}\right)^{1/3} k M_*^{2/3} \tag{8}$$

From this relation, the exoplanet mass can be derived.

2.3 Markov-Chain Monte Carlo (MCMC) Sampling

In this work, *Markov Chain Monte Carlo* (MCMC) algorithms are used in order to better fit the data. First, it is important to define what Markov Chains and Monte Carlo simulations are, respectively. In a general sense, *Markov Chains* are a sequence of possible events where the probability of each event depends only on the state achieved in the previous state. *Monte Carlo simulations* are a broad class of algorithms that utilize repeated random sampling in order to obtain some numerical results [20].

Essentially, these algorithms start with a prior distribution (i.e. an initial estimate about the parameters). Then, they iteratively update parameter estimates by sampling from the observed data. This process involves running multiple Markov chains, where each chain is a sequence of parameter values that evolve over iterations. At each step, a new set of parameters is proposed and then accepted or rejected based on a criterion, which is discussed in a later section, that ensures the chain converges to the posterior distribution. After some time of sampling, the remaining samples approximate the true posterior distribution, allowing for statistical inference about the parameters' likely values and uncertainties. It should also be noted that the posterior distribution describes the values of all the target parameters, the algorithm is not ran for individual parameters.

In the context of this work, the quantities that the MCMC algorithm finds are the parameters associated with the exoplanet and its host star. For instance, in the case of transit data, the algorithm can find the best value for the radius of the planet. On the other hand, in the case of RV data, the algorithm can find the most optimal value for the mass of the planet. Other parameters are calculated by this algorithm, such as the orbital period, semi-major axis of the obit, eccentricity of the orbit, etc.

2.4 pyexofits Library

The main tool used in the analysis of data in this project is the `pyexofits`. This is a Python library developed by one of the greater GEMS project leads, Dr. Shubham Kanodia. This library takes in data from telescopes, such as HPF or TESS, and fits a model to the data.

It utilizes MCMC algorithms to fit this model to the data. It then produces a file known as a "Chain Summary". This summary files tells the user if the MCMC algorithm has run successfully or not. This file also contains all the parameters that were calculated (i.e. the mass of the planet). The value that determines whether the chains have converged (i.e. that the value is a correct value) is known as the "Rhat" value. If this value is less than 1.05, then it can be said that the chains successfully converged on the listed value [21].

Two other parameters also dictate the validity of the posterior model values generated, these are the `ess_bulk` and `ess_tail`, which are the bulk effective sample size and the tail effective sample size, respectively. The `ess_bulk` value tells the sampling efficiency, thus it is indicative of the efficiency of the mean and median estimates. The `ess_tail` value is indicative of the measure of the sampling efficiency at the ends of the distribution [21].

Both of these values should be at least 100 per chain [21]. It should be noted that MCMC fits should be run with at least four chains being used [21]. This helps to ensure that the values in the posterior distribution that are produced are as accurate as they can be.

The main script used from this library is the `xo_JointFitting.py`. This script takes in data from transit data sources (such as TESS) and from RV data sources (such as HPF) and uses all of this data to find many of the target parameters in one go. When this script was used, data from TESS and HPF were used exclusively. This script also produces plots by curve fitting the data with the calculated posterior distribution.

3 Data

3.1 TESS Instrument Details

The first of the two instruments utilized in this work is the TESS space telescope. As was briefly described above, TESS, or the *Transiting Exoplanet Survey Satellite*, is a space telescope created by NASA. Its main mission is to monitor on the order of 200,000 main sequence stars, looking for exoplanet transits [16]. It serves as a follow-up of sorts to the Kepler mission. However, unlike Kepler, TESS has an all-sky coverage.

TESS has four identical wide-view CCD cameras, each with a 24° by 24° field of view [16]. Thus, the whole field of view is 24° by 96° , or 2,300 deg^2. Each CCD camera has an imaging array of 2,048 by 2,048 sensors. These CCD cameras produce images with exposure times of 2 seconds, which are summed into groups of 60 frames. This creates an effective exposure of 2 minutes. The full frame images are then down linked every 30 minutes [16].

The entire survey region is divided into 26 sectors, with 13 sectors per hemisphere. Each TESS sector spans the entire field of view of the instrument, that being a 24° by 96° region. Each of these sectors are observed for about 27.4 days. As such, an all sky survey can be completed in a little less than 2 years (about 712 days) [16].

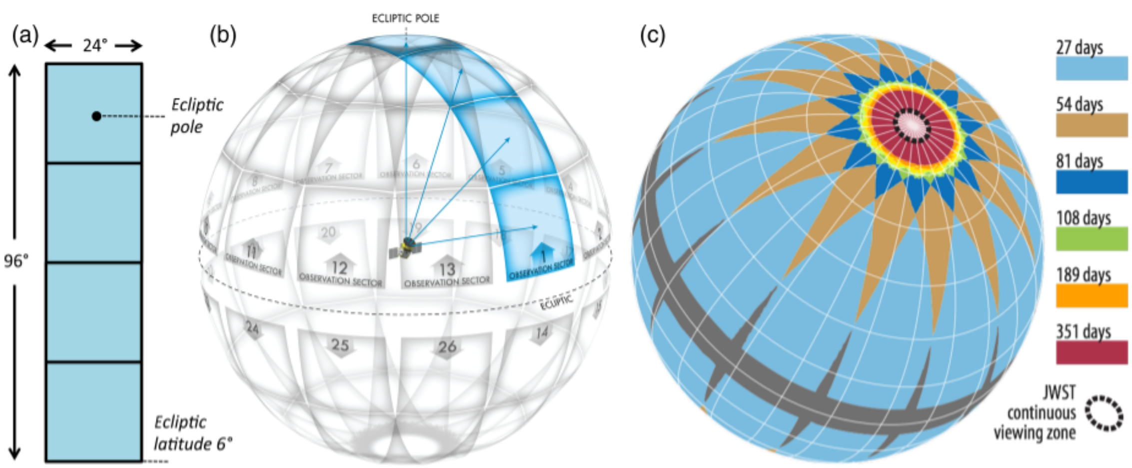

Figure 3: (a) Shows the full field of view of the four CCD cameras. (b) Shows the division of the sky into the 26 sectors for observation. (c) The duration of observations on the sky, noting the overlap between sectors. Also note the black dashed line at the pole, which is a region that JWST can observe at any time. [16]

TESS also has an elliptical orbit with a period of 13.7 days. The instrument orbits with a perigee of about $17R_{\oplus}$ and an apogee of about $59R_{\oplus}$.

3.2 TESS Transit Data

In this work, data from transit data for the system was used and analyzed. This data contains the time of the observation (in BJDTDB), the measured flux values of the star, and the error of the flux measurement. These values are stored in a CSV file so they can be easily read The data file contains 2,822 data points in total, in order to ensure plenty of data was taken over time. The time that the data was taken over is about 27.2 days.

Note that BJDTDB refers to the *Barycentric Julian Date* (BJD) with the*Barycentric Dynamical Time* (TDB). The former is the typical Julian date but with corrections implemented to account for the position of the Earth with respect to the center of mass of the solar system, while the latter is a timescale that takes relativistic accounts into consideration.

3.3 HPF Instrument Details

The HPF, or *Habitable-Zone Planet Finder*, is a near-infrared (NIR) spectrograph instrument designed to be used with the Hobby-Eberly Telescope (HET), which is a ground based telescope in Davis Mountains, Texas [22]. The primary goal of this instrument is to detect exoplanets around M-type dwarf stars through measuring their radial velocities [22]. HPF was designed to target these M-type dwarf star systems because these stars have a relatively low luminosity and the orbital periods of habitable zone planets are typically short. These types of stars also emit the majority of their flux in the NIR part of the spectrum, so HPF is an ideal tool for this kind of observation [22].

The actual HPF spectrograph is housed in a vacuum vessel, a cryostat, cooled to about 200k with a heat sink that utilizes liquid nitrogen to ensure the instrument stays cool. The vacuum sealing and the cool temperature helps to mitigate any background radiation that the spectrograph could pick up. This cryostat ensures a temperature stability of < 10mK [22].

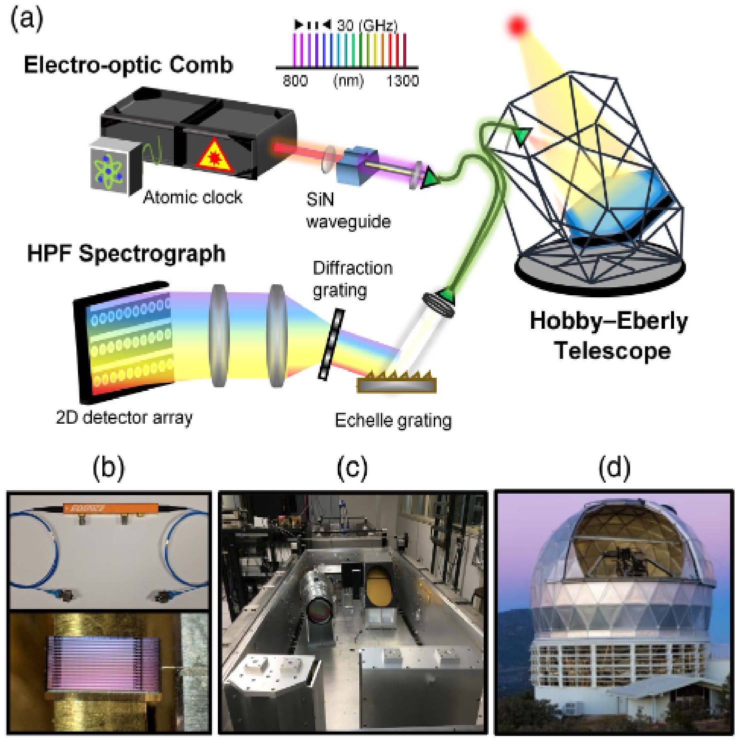

Figure 4: (a) A diagram of the actual HPF instrument and how it connects to the HET. (b) Components of the frequency comb generator, a fiber-optic modulator (top) and a silicon nitride chip (bottom). (c) The actual HPF instrument itself, opened up. (d) The HET at the McDonald Observatory in Texas. [22]

The instrument collects light from the HET with a 300 μm fiber subtends an angle of 1.7 arcsec and a 200 μm fiber subtends an angle of 1.13 arcsec. One of these fibers is used for calibrating the spectrograph, while the other is used to actually observe the celestial objects [22]. Calibrating the spectrograph is done with lamps of certain elements in order to set a baseline for what should be observed. HPF uses 200 by 800 mm echelle gratings (a type of diffraction grating used in high resolution spectroscopy) arranged in a mosaic, which function as one large grating. These grating break the incident light into its spectral lines, thus allowing the detector array to monitor the spectrum for any Doppler shifts from the baseline spectral lines [22].

The HPF targets M mid to late M dwarfs (M4 to M9) within 33 parsecs of Earth [22]. It emphasizes stars with a low rotational velocity (i.e. $|v|\sin(i) < 12$km/s) which ensure higher precision RV measurements. The initial sample includes about 300 stars, with 50 promising targets selected for further observation.

3.4 HPF RV Spectroscopy Data

In this work, data from the HPF detector was also used. This data contains the time observed (again in BJDTDB), the measured RV value, and the error in the measured value. The data file used in this work is a CSV file and contains only about 13 points due to the fact that only binned data was considered in this work. These 13 data points were collected over a time interval of approximately 75.5 days. The measured RV values were computed from the shifts in the stellar spectrum that HPF observed using a modified version of the SERVAL (SpEctrum Radial Velocity AnaLyzer) pipeline [23].

4 Results & Analysis

4.1 TESS Photometry Fits

We begin by looking at the results generated by running the MCMC algorithm on the provided TESS data. This data shows that the planet, TOI-5916b, does indeed exhibit transits across its host star.

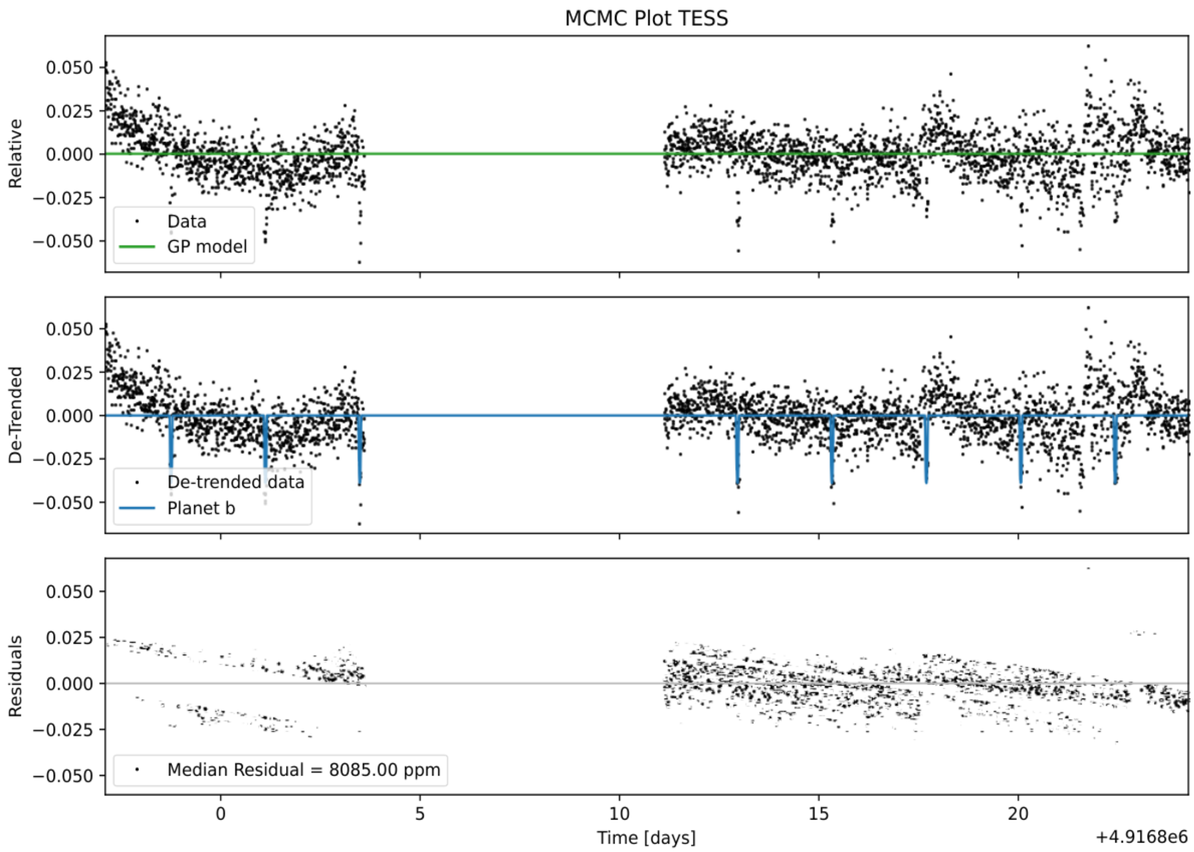

Figure 5: TESS Flux data, where the transits made by the planet are prominently shown in the blue masking in the second frame. The times when there is no data presents represents a time interval over which the telescope was not taking data.

Notice the distinct drops in the relative flux that appear to be periodic over time. This plot can help us to determine the period of the planet's orbit around the host star, as the occurrence of these periodic drops in flux is indicative of when the planet transits in front of the star. Thus, by eyeing these plots, we can see that the period of the planet around its host star is ≈ 2.5 days or so.

We can also look at the relative light curve that the code used created. This curve represents the relative dip in the brightness of the star.

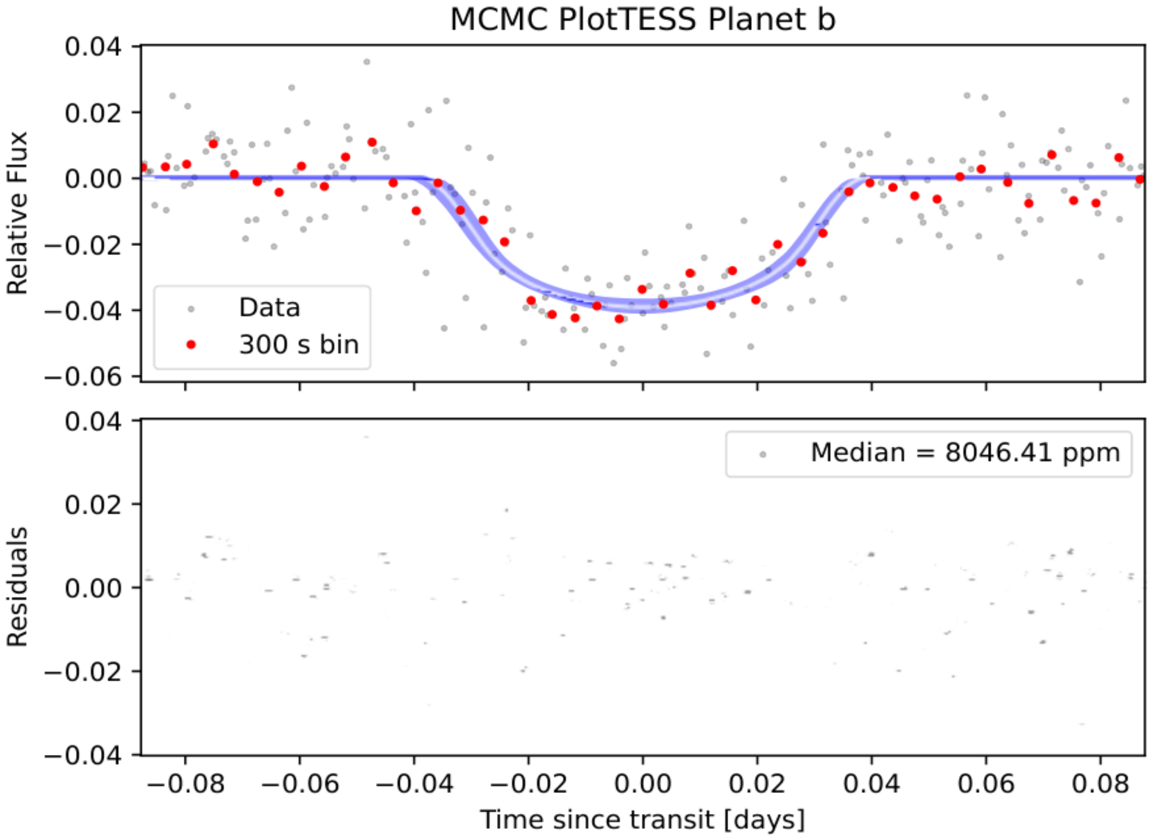

Figure 6: The drop in flux over time relative to the initial brightness of the star, which we set to zero as a baseline.

This curve shows us the factor by which the star's brightness has fallen. This quantity, which was discussed earlier, is known as the transit depth. By eying the plot once again, it can be seen that the transit depth is ≈ 0.04 or 4%. That is, the observed stellar flux decreases by about 4% whenever the planetary system transits in front of it.

4.2 HPF RV Fits

Now, we can look at the RV data from the HPF detector. This data shows us what the max and min radial velocities are, and also helps us to confirm the value of the period obtained from the transit data, and to find the mass of the planet, among other things.

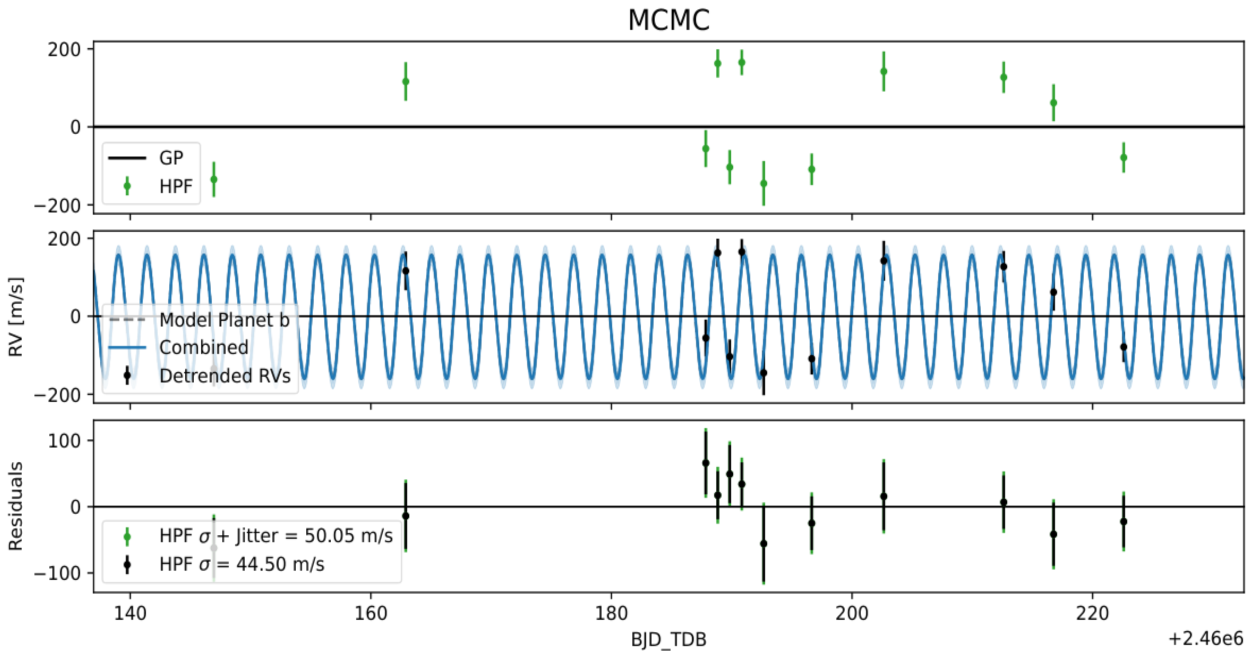

Figure 7: The top plot shows the raw RV data points relative to the zero baseline. The second plot shows the model that the MCMC algorithm has fit to the data points.

From eyeing this plot, it can be seen that the amplitude of the radial velocity is somewhere slightly less than 200 m/s. However, while this is easy to see from this plot, the period is a value that is not as easy to see. The code used then created a phase folded version of this plot. That is, a plot that shows the radial velocity as a function of the orbital phase, rather than as a function of the time of observation, where we can clearly see the amplitude value and the period itself.

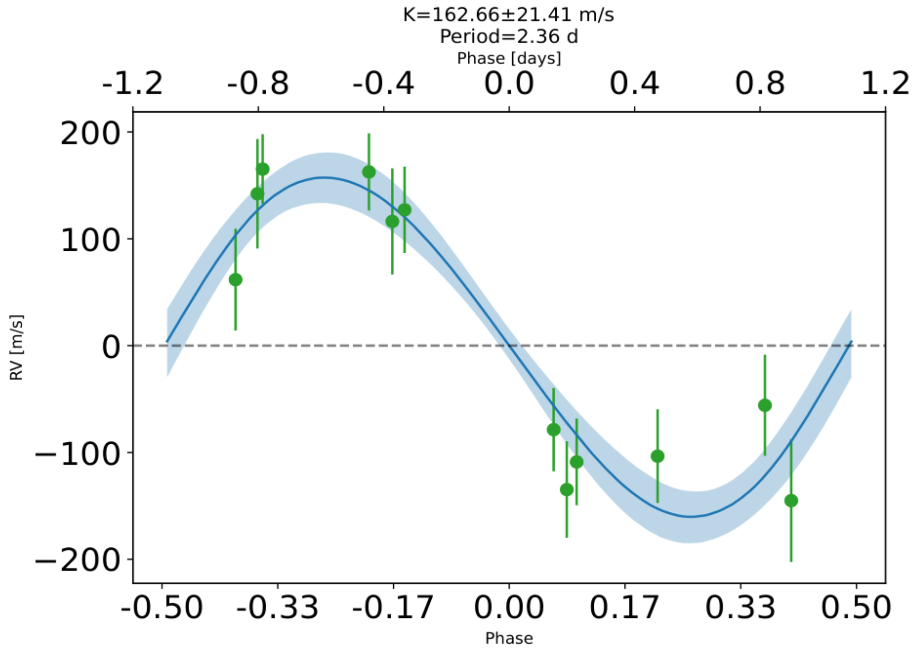

Figure 8: Shows the phase folded RV curve, where the bottom axis is the phase, the top axis is the time in days, and the left side axis is the radial velocity in m/s.

From this phase folded plot, just eying it, it can be easily seen that the period for the shift in the radial velocity is about 2.4 days. This lines up with the data that the transit fit showed previously. Other parameters, such as the mass of the planet, can be calculated by the looking at the amplitude of this curve.

4.3 Posterior Distribution Values & Analysis

The MCMC algorithm used also calculated values that are not as easily shown on the plots. Some of the most important values that the algorithm calculated are tabulated below. These values make up the posterior distribution that the sampling algorithm had set out to find.

Parameter	**Mean**	**Std. Dev.**	`ess_bulk`	`ess_tail`	`r_hat`	**Median**
R_* $(R_\odot)$	0.469	0.015	7001	5945	1	0.496
$M_*(M_\odot)$	0.481	0.021	6852	6511	1	0.481
T_{eff} (K)	4,002.1	98.879	7585	6260	1	4001.956
k (m/s)	162.645	22.896	5869	4322	1	162.656
P (Days)	2.365	≈ 0	3440	3186	1	2.365
R_{pl}/R_*	0.194	0.064	2338	1229	1	0.174
r_{pl} $(R_\oplus)$	10.57	0.139	2325	1214	1	10.57
M_{pl} $(M_\oplus)$	206.312	29.345	6009	4079	1	206.47
ρ_{pl} (g/cm^3)	1.41	0.835	2357	1207	1	1.339

Table 3: Table of some of the notable parameters calculated for the posterior distribution.

Noting that the recommended four chains were used for the MCMC sampling, we can easily see that the `ess_bulk`, `ess_tail`, and `r_hat` values are all within the acceptable ranges as described previously. Thus, we can trust that these values have converged to accurate values for the provided data.

5 Discussion

5.1 What Can be Learned

From posterior distribution data table, we can easily discern a lot of information about the system. We now know that the system TOI-5916 is a gaseous planet ($\rho_{\text{pl}} = 1.41$ g/cm^3), has a radius of about 10 times that of the Earth, and has a mass of about 206 times that of the Earth. In terms of the Jovian (Jupiter) radius and mass, this works out to be about 0.892 times the radius of Jupiter, and about 0.648 times the mass of Jupiter. The plotted values for the radial velocity and the orbital period have also been confirmed as 162.645 ± 22.9 m/s and 2.365 days, respectively.

5.2 Methods for Improvement

Although the values in the provided table seem to converge to the correct values, a follow-up study of the system should be conducted to ensure that the values that were converged to were accurate and correct.

It should be noted that the script used for the MCMC sampling, `xo_JointFitting.py`, has the ability to increase the precision of the measurements by incorporating data from ground based transit observations. In this study, a ground based transit was not used, and thus using such data in a future follow-up study could improve the accuracy of the measured parameters.

It should also be noted that the MCMC algorithm reported the value for the orbital period as having an error of ≈ 0. Although this is unusual, when checked with the other computed values this value for the orbital period seems to be correct. This is most likely due to a rounding issue, where the number was so small it was rounded to 0 in the chain summary table.

6 Conclusion

In summary, data for the system TOI-5916b were collected from the TESS and HPF telescopes. This data was then run through an MCMC sampling algorithm, from the Python library `pyexofits`, which read the data and determined the parameters of interest as well as some plots. These values were then collected and tabulated so that the planet could be characterized.

In conclusion, the exoplanet TOI-5916b was confirmed to be a giant exoplanet ($r_{pl} = 10.57M_{\oplus}$) with a gaseous composition ($\rho_{pl} = 1.41\text{g/cm}^3$). It has a mass of $206.3M_{\oplus}$, a period of $P = 3.265$ days, and it causes its host star to wobble with a radial velocity amplitude of $k = 162.65$m/s. We can also see that the host star has an effective temperature of about $4,000$K and thus is indeed an M-type dwarf star.

7 References

[1] *Overview — What is an Exoplanet?* Exoplanet Exploration: Planets Beyond our Solar System. URL: https://exoplanets.nasa.gov/what-is-an-exoplanet/overview (visited on 05/30/2024).

[2] A. Wolszczan and D. A. Frail. "A planetary system around the millisecond pulsar PSR1257 + 12". In: 355.6356 (Jan. 1992), pp. 145–147. DOI: 10.1038/355145a0.

[3] Michel Mayor and Didier Queloz. "A Jupiter-mass companion to a solar-type star". In: 378.6555 (Nov. 1995), pp. 355–359. DOI: 10.1038/378355a0.

[4] R. Paul Butler et al. "Evidence for Multiple Companions to υ Andromedae". In: 526.2 (Dec. 1999), pp. 916–927. DOI: 10.1086/308035.

[5] James F. Kasting, Daniel P. Whitmire, and Ray T. Reynolds. "Habitable Zones around Main Sequence Stars". In: 101.1 (Jan. 1993), pp. 108–128. DOI: 10.1006/icar.1993.1010.

[6] Slavek Rucinski et al. "Most (Microvariability & oscillations of stars) Canadian astronomical micro-satellite". In: *Advances in Space Research* 31.2 (Jan. 2003), pp. 371–373. DOI: 10.1016/S0273-1177(02)00628-2.

[7] M. W. Werner et al. "The Spitzer Space Telescope Mission". In: 154.1 (Sept. 2004), pp. 1–9. DOI: 10.1086/422992. arXiv: astro-ph/0406223 [astro-ph].

[8] David Charbonneau et al. "Detection of Thermal Emission from an Extrasolar Planet". In: 626.1 (June 2005), pp. 523–529. DOI: 10.1086/429991. arXiv: astro-ph/0503457 [astro-ph].

[9] *MOST satellite Archives*. Universe Today. June 16, 2020. URL: https://www.universetoday.com/tag/most-satellite/ (visited on 06/08/2024).

[10] *Historic Timeline — Explore*. Exoplanet Exploration: Planets Beyond our Solar System. URL: https://exoplanets.nasa.gov/alien-worlds/historic-timeline (visited on 05/30/2024).

[11] William J. Borucki et al. "Kepler Planet-Detection Mission: Introduction and First Results". In: *Science* 327.5968 (Feb. 2010), p. 977. DOI: 10.1126/science.1185402.

[12] François Fressin et al. "Kepler-10 c: a 2.2 Earth Radius Transiting Planet in a Multiple System". In: 197.1, 5 (Nov. 2011), p. 5. DOI: 10.1088/0067-0049/197/1/5. arXiv: 1105.4647 [astro-ph.EP].

[13] Elisa V. Quintana et al. "An Earth-Sized Planet in the Habitable Zone of a Cool Star". In: *Science* 344.6181 (Apr. 2014), pp. 277–280. DOI: 10.1126/science.1249403. arXiv: 1404.5667 [astro-ph.EP].

[14] N. C. Santos et al. "The CORALIE survey for southern extra-solar planets VI. New long period giant planets around HD 28185 and HD 213240". In: 379 (Dec. 2001), pp. 999–1004. DOI: 10.1051/0004-6361:20011366.

[15] Steve B. Howell et al. "The K2 Mission: Characterization and Early Results". In: 126.938 (Apr. 2014), p. 398. DOI: 10.1086/676406. arXiv: 1402.5163 [astro-ph.IM].

[16] George R. Ricker et al. "Transiting Exoplanet Survey Satellite". In: *Journal of Astronomical Telescopes, Instruments, and Systems* 1.1 (2014), p. 014003. DOI: 10.1117/1.JATIS.1.1.014003. URL: https://doi.org/10.1117/1.JATIS.1.1.014003.

[17] *TESS_alone_high_res.jpg (JPEG Image, 6016 × 4016 pixels) — Scaled (18%)*. URL: https://svs.gsfc.nasa.gov/vis/a010000/a012700/a012782/TESS_alone_high_res.jpg (visited on 05/30/2024).

[18] Mahima Kaushik, Aditee Mattoo, and Ritesh Rastogi. *Exoplanet Detection : A Detailed Analysis*. 2024. arXiv: 2404.09143 [astro-ph.EP].

[19] Shubham Kanodia et al. "Searching for Giant Exoplanets around M-dwarf Stars (GEMS) I: Survey Motivation". In: 167.4, 161 (Apr. 2024), p. 161. DOI: 10.3847/1538-3881/ad27cb. arXiv: 2402.04946 [astro-ph.EP].

[20] Thomas Wiecki. *while my_mcmc: gently(samples) - MCMC sampling for dummies*. Nov. 10, 2015. URL: https://twiecki.io/blog/2015/11/10/mcmc-sampling/ (visited on 06/04/2024).

[21] *Convergence and efficiency diagnostics for Markov Chains — Rhat*. URL: https://mc-stan.org/rstan/reference/Rhat.html (visited on 06/14/2024).

[22] Suvrath Mahadevan et al. "The habitable-zone planet finder: a stabilized fiber-fed NIR spectrograph for the Hobby-Eberly Telescope". In: *Ground-based and Airborne Instrumentation for Astronomy IV*. Ed. by Ian S. McLean, Suzanne K. Ramsay, and Hideki Takami. Vol. 8446. Society of Photo-Optical Instrumentation Engineers (SPIE) Conference Series. Sept. 2012, 84461S, 84461S. DOI: 10.1117/12.926102. arXiv: 1209.1686 [astro-ph.EP].

[23] Gudmundur Stefansson et al. "A Sub-Neptune-sized Planet Transiting the M2.5 Dwarf G 9-40: Validation with the Habitable-zone Planet Finder". In: 159.3, 100 (Mar. 2020), p. 100. DOI: 10.3847/1538-3881/ab5f15. arXiv: 1912.00291 [astro-ph.EP].